The Astronomical Journal, 128:2954–2961, 2004 December

H I GAS IN HIGHER DENSITY REGIONS OF THE INTERGALACTIC MEDIUM[1]

Toru Misawa,[2] David Tytler,[3,4] Masanori Iye,[5,6] Pascal Paschos,[3] Michael Norman,[3] David Kirkman,[3,4] John O'Meara,[3,4] Nao Suzuki,[3,4] and Nobunari Kashikawa[5]

Received 2004 May 11; accepted 2004 September 8

ABSTRACT

Using H I absorption alone, we attempt to separate H I absorption lines in quasar spectra into two categories: higher density lines (HDLs) and lower density lines (LDLs), and we discuss the difference in their physical properties. We deblend and fit all H I lines with Voigt profiles and make an unbiased sample of H I lines covering a wide column density range ($12 < \log N_{\rm H\,I}\ [{\rm cm}^{-2}] < 19$). To reduce the influence of line blending, we simultaneously fit several Lyman series lines. As a result of a two-point correlation analysis, we found that higher column density H I lines are clustering at $\Delta v < 200$ km s^{-1}, whereas lower ones cluster at $\Delta v < 100$ km s^{-1}. We define HDLs as H I lines with $15 < \log N_{\rm H\,I} < 19$ and all H I lines within 200 km s^{-1} of a line with $\log N_{\rm H\,I} > 15$ and LDLs as all others with $12 < \log N_{\rm H\,I} < 15$. We found that the HDLs have smaller minimum b-values for a given column density than the LDLs. This difference is successfully reproduced by our hydrodynamic simulation. The LDLs seem to be cool or shock-heated diffuse intergalactic medium gas, whereas the HDLs are likely to be cooler dense gas near to galaxies.

Key words: galaxies: ISM — intergalactic medium — quasars: absorption lines

1. INTRODUCTION

Quasars have been used as background sources, allowing the study of objects that lie between us and them, most of which make Lyα absorption lines. To date, line-profile fitting analysis for Lyα absorption lines has been carried out to study physical parameters such as the velocity width and the column density (Pettini et al. 1990; Carswell et al. 1991; Rauch et al. 1992; Hu et al. 1995, hereafter H95; Lu et al. 1996b, hereafter L96; Kirkman & Tytler 1997, hereafter KT97).

Samples of H I absorption lines usually contain (1) H I lines originating in the intergalactic diffuse gas and (2) H I lines produced near or in intervening galaxies. The former could be weak H I lines widely distributed as the Lyα forest (hereafter, we call these lower density lines [LDLs]), whereas the latter are likely to be strong H I lines clustered as metal absorption lines (hereafter, we call these higher density lines [HDLs]). HDLs are thought to be caused by discrete clouds. On the other hand, LDLs probably arise from photoionized intergalactic medium (IGM) in the continuous density fields that are broadened by Hubble flow (e.g., Rauch 1998; Kim et al. 2002a). Here, the reader can think of density as column density $N_{\rm H\,I}$ or volume density, since numerical simulations show that the two are correlated (Zhang et al. 1998). The HDLs are lines formed in or near higher density parts of the IGM. As the $\log N_{\rm H\,I}$ increases, especially above about 17, these regions are more likely to be in or near the outer parts of galaxies or clumps that will become galaxies. In contrast, the LDLs arise in relatively lower density regions of the IGM.

There are studies that suggest that some H I absorption lines have a close relationship with galaxies near the line of sight, not only on small scales at low z (Grogin & Geller 1998; Penton et al. 2002), but also on large scales at high z (Adelberger et al. 2003). McDonald et al. (2002) presented theoretical predictions of the correlation between the Lyα forest transmitted flux and the mass of absorbers within $\sim 5\ h^{-1}$ Mpc (comoving) of the line of sight. Other spectroscopic and imaging observations have been carried out in order to study the statistical relationship between the Lyα absorbers and galaxies at low z. The most important result is that the Lyα equivalent widths are anticorrelated with the projected distance of the nearest galaxies within $500\ h^{-1}$ kpc of the galaxies (Lanzetta et al. 1995; Tripp et al. 1998; Davé et al. 1999; Chen et al. 2001). Thus, some H I absorbers seems to be closely related with galaxies.

Therefore, the analysis of HDLs and LDLs is indispensable for the detailed investigation of physical properties of H I gas. However, one of the most serious problems in such an analysis is that the Lyα absorption lines are so heavily blended with each other that it is difficult to separate and fit them individually. This problem is often seen in strong H I lines with $\log N_{\rm H\,I} > 15$ (cm^{-2}).

In some past studies, the column densities of strong H I lines have been evaluated using the Lyman limit optical depth for Lyman limit systems (LLSs), or the total rest-frame equivalent width for damped Lyα (DLA) systems without fitting them by Voigt profiles (e.g., Lanzetta et al. 1991; Petitjean et al. 1993). These methods, however, evaluate only the total column densities and Doppler parameters of the heavily blended H I lines.

In this study, we attempt to fit all H I lines with Voigt profiles, construct an unbiased sample of H I lines over a wide column density range ($12 < \log N_{\rm H\,I} < 19$), and investigate their physical parameters, such as column density, Doppler parameter, and clustering properties. In order to separate the

[1] Data presented herein were obtained at the W. M. Keck Observatory, which is operated as a scientific partnership among the California Institute of Technology, the University of California, and the National Aeronautics and Space Administration. The Observatory was made possible by the generous financial support of the W. M. Keck Foundation.

[2] Department of Astronomy and Astrophysics, Pennsylvania State University, University Park, PA 16802; misawa@astro.psu.edu.

[3] Center for Astrophysics and Space Sciences, MS 0424, University of California at San Diego, 9500 Gilman Drive, La Jolla, CA 92093-0424.

[4] Visiting Astronomer, W. M. Keck Observatory which is a joint facility of the University of California, the California Institute of Technology, and NASA.

[5] National Astronomical Observatory, 2-21-1 Osawa, Mitaka, Tokyo 181-8588, Japan.

[6] Department of Astronomical Science, The Graduate University for Advanced Studies, 2-21-1 Osawa, Mitaka, Tokyo 181-8588, Japan.

heavily blended (strong) H I lines and fit them individually with Voigt profiles, we use not only the Lyα line but also higher Lyman series lines, such as Lyβ and Lyγ, to improve the fitting accuracy.

This method has previously been applied to only a few LLS and DLA systems (e.g., Songaila et al. 1994; Tytler et al. 1996; Wampler et al. 1996; Carswell et al. 1996; Songaila et al. 1997; Burles & Tytler 1998a, 1998b; Burles et al. 1999; Kirkman et al. 2000; O'Meara et al. 2001; Kirkman et al. 2003) and to the Lyα forest in two quasar spectra (Kim et al. 2002a). Here we apply this fitting method to 40 quasar spectra acquired with the Keck HIRES (Vogt et al. 1994).

Finally, we attempt to separate H I lines into HDLs and LDLs and apply our statistical analysis to these two classes separately. We confirm that the column density distribution and the Doppler parameter distribution of LDLs are similar to the past results (H95; L96; KT97). We found the most remarkable difference between HDLs and LDLs in the plot of column density versus Doppler parameter, which suggests that H I absorbers are not produced by a single phase (or a single population). This difference is also reproduced by our hydrodynamic simulation. The summary of the other results and the detailed description of each absorption system are presented in Misawa et al. (2004).

We give a brief description of the observation in § 2. In § 3, we explain how to evaluate the line parameters. In § 4, we investigate the physical properties of HDLs and LDLs and compare the observational results with the hydrodynamic simulation. We summarize our results in § 5.

2. OBSERVATIONS

The sample quasars were originally selected from a survey taken for measurements of the D/H (deuterium to hydrogen) abundance ratio. The typical ratio of D/H is so small, 3×10^{-5} (Kirkman et al. 2003 and references therein), that we can only detect D I lines corresponding to H I lines with large column densities, $\log N_{\rm H\,I} \geq 16.5$. Given this fact, we observed quasars in which either DLA systems or LLSs were detected. Here we examine Keck HIRES spectra of 40 quasars. We used a 1.″14 slit, which provided a resolution of 8.0 km s^{-1}. The spectra were extracted by the automated MAKEE program written by T. Barlow.

3. PREPARATION OF UNIFORM SAMPLE

Instead of detecting all of the H I lines in the spectra of the 40 quasars, this study includes only the H I lines with $\log N_{\rm H\,I} > 15$ and all other H I lines within 1000 km s^{-1} of such H I lines. The reason is described below.

3.1. *Detection of* H I *Systems*

We at first searched for H I lines with $\log N_{\rm H\,I} > 15$ in the following way: (1) we found H I lines already discovered in DLA systems or LLSs in earlier work (Sargent et al. 1989; Lanzetta 1991; Tytler 1982; Burles 1997), (2) we checked for H I lines corresponding to previously discovered metal absorption systems (Péroux et al. 2001; Storrie-Lombardi et al. 1996; Petitjean et al. 1994; Lu et al. 1993; Steidel & Sargent 1992; Lanzetta et al. 1991; Barthel et al. 1990; Steidel 1990; Sargent et al. 1980, 1988), and (3) we finally attempted to detect H I lines ourselves that satisfied both of the following conditions: (*a*) the H I line has a column density of $\log N_{\rm H\,I} \geq 15$ and (*b*) at least one higher Lyman series, e.g., Lyβ and Lyγ lines, is present along with Lyα in the observed wavelength range, which improves the reliability of line fitting. We do not consider metal lines.

Metal absorption lines (Sargent et al. 1980, 1988; Young et al. 1982; Petitjean & Bergeron 1994; Churchill & Vogt 2001; Pichon et al. 2003), including those in DLA systems (Lu et al. 1996a), cluster at $\Delta v < 400$ km s^{-1}. It is then sufficient to detect all lines within 1000 km s^{-1} of the H I lines with $\log N_{\rm H\,I} > 15$ for the purpose of studying the physical properties of weak and strong H I lines. When more than one H I line with $\log N_{\rm H\,I} > 15$ was detected within this velocity window, the position of the line with the largest column density (hereafter the "main H I component") was considered to be the center of the H I system. As an example, we show the velocity distribution of H I lines for the system at $z_{\rm abs} = 3.321$ in the spectrum of Q0014+8118 in Figure 1 (see also Burles et al. 1999). With this method, we detected 86 H I systems at $2.1 < z < 4.0$ in the spectra of 31 quasars out of a total of 40 examined.

3.2. *Evaluation of Line Parameters*

For the fitting of each absorption line with a Voigt profile, we fitted all the accessible lines in the Lyman series, helping us deblend H I lines and make an unbiased sample of H I lines. In the process of line detection, we removed very narrow lines with Doppler parameters of $b < 4.81$ km s^{-1} or FWHM $\sim$8.0 km s^{-1}, which is the resolution of our spectra. We decided to ignore all lines with $b < 15$ km s^{-1}, as described later. If the Voigt fitting allowed different solutions during the fitting trials, the result with the minimum number of lines was chosen. This occurs mainly in the saturated region for which we have only a small number of Lyman series information. If we fitted the line profiles using a smaller number of components than the actual number, the *b*-values could be overestimated. On the other hand, the column density cannot be easily overestimated, because only a small rise of the column density significantly changes the line profiles (e.g., damping profile), especially at the saturated regions.

Once the fitting model was applied to the absorption lines in some region of the spectra, we used χ^2 minimization to find the model parameters that best fitted the observed spectrum. The formal errors on the fitted parameters for lines with $b < 30$ km s^{-1} are $\sigma(\log N_{\rm H\,I}) = 0.09$, $\sigma(b) = 2.1$ km s^{-1}, and $\sigma(z) = 2.5 \times 10^{-5}$. Before beginning our statistical analysis, we prepared an unbiased sample of H I lines by eliminating inappropriate H I systems that have disadvantages as described below.

1. *Poor fitting because of gaps in echelle-formatted spectra*.—Echelle-formatted spectra sometimes have data gaps between echelle orders. This occurs frequently in the redder part of the spectrum (e.g., $\lambda > 5000$ Å in our data). Spectral gaps appear about every 100 Å, and the widths of the wider gaps are no less than 20 Å depending on the wavelength. If the Lyman series line damaged by the spectral gaps is Lyα, the fitting accuracy for the system is very low. Therefore, we removed H I systems whose Lyα lines are affected by spectral gaps wider than 100 km s^{-1}.

2. *Poor fitting because of strong DLA wings*.—DLA (and sub-DLA) systems with large H I column densities of $\log N_{\rm H\,I} \geq 19$ are unsuitable for our study, not only because their absorption profiles are damped so strongly that almost all weak components are blanketed by the damping wings, but also because the spectra around DLA lines are not normalized correctly because of the strong absorption features.

3. *Close proximity in redshift to the background quasars*.—The Lyα forest disappears in the regions redward of

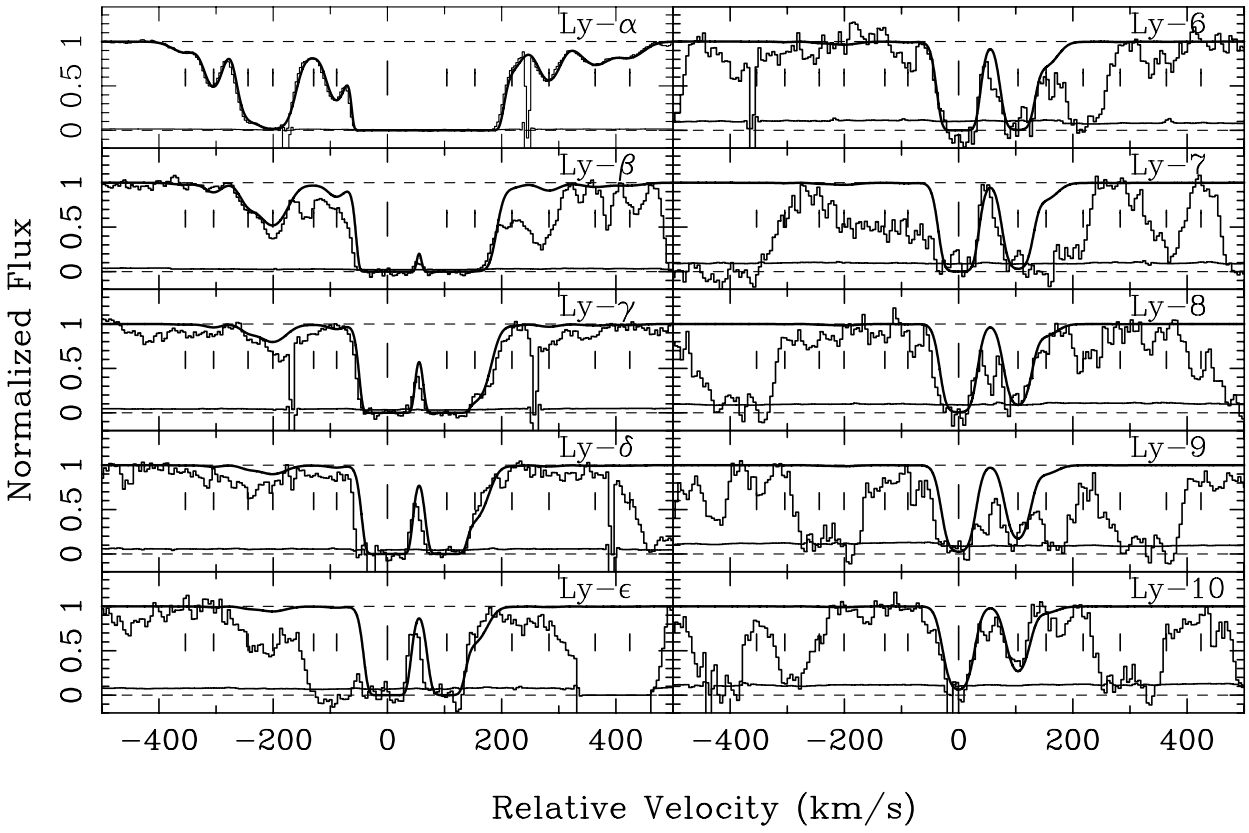

FIG. 1.—Observed and modeled velocity map for 10 Lyman series lines of the H I at $z_{abs} = 3.321$ in the spectrum of Q0014+8118. The lower line in each panel is the 1 σ error. Tick marks denote the positions of H I absorption lines, and the large one at the center is the position of the main component.

the Lyα emission lines of the quasars. Therefore, we remove H I systems at a distance of $\leq$1000 km s^{-1} from the Lyα emission lines, because the asymmetrical distribution of their H I lines complicates the clustering analysis described in § 4.1.

4. *Overlapping with other* H I *systems*.—H I system pairs whose velocity windows of $\pm$1000 km s^{-1} overlap are also excluded, since their distribution of H I lines could affect each other and the line clustering analysis is contaminated.

Finally, we have an unbiased sample of 973 H I lines in 61 H I systems. However, the sample is not homogeneous, because the signal-to-noise (S/N) ratio varies. The S/N ratios of the spectra are at least S/N $\simeq$ 11 per 2.1 km s^{-1} pixel, and the mean value is S/N $\simeq$ 47 for Lyα lines.

4. PHYSICAL PROPERTIES OF H I LINES

We used the sample prepared in § 3 to study the H I line parameters. Our analysis is similar to that of previous studies (e.g., H95; L96; KT97), but with three key differences: (1) earlier studies used all H I lines detected in the quasar spectra, whereas we use only H I lines within 1000 km s^{-1} of the main components with $\log N_{\rm H\,I} > 15$, (2) our sample contains a number of strong H I lines ($\log N_{\rm H\,I} > 15$) in addition to weak lines ($\log N_{\rm H\,I} < 15$), and (3) our sample covers a wide redshift range, $2.0 \leq z \leq 4.0$, compared with those of the past studies, in which $\Delta z \sim 0.5$.

4.1. *Clustering Properties*

Our sample contains not only LDLs but also HDLs. Davé et al. (1999) noted in their hydrodynamic simulations that galaxies tend to lie near the dense regions that are responsible for strong H I lines. Therefore, we attempted to classify the lines using their clustering along the line of sight by constructing the two-point correlation function (Sargent et al. 1980),

$$\xi(v) = \frac{N(v)}{N_{\rm exp}(v)} - 1, \quad (1)$$

where $N(v)$ is the number of observed pairs at a velocity separation of v and $N_{\rm exp}(v)$ is the number of line pairs expected if they are randomly placed along the line of sight. The value of $N_{\rm exp}(v)$ is calculated by Monte Carlo simulations. Webb (1987) found significant clustering, $\xi(v) = 0.32 \pm 0.08$ over the velocity range 50 km s^{-1} $< v <$ 150 km s^{-1} at $1.9 < z < 2.8$. H95 confirmed the same trend with $\xi(v) = 0.17 \pm 0.045$ over the same velocity range at $\langle z \rangle = 2.8$. With a large sample of H I lines with $\log N_{\rm H\,I} > 13.8$ at $1.7 < z < 4.0$, Cristiani et al. (1997) also found that the correlation function at $v \sim 100$ km s^{-1} increases with $\log N_{\rm H\,I}$. On the other hand, Rauch et al. (1992), L96, and KT97 did not find any clustering for similar velocity ranges at $2.7 < z < 3.4$, $\langle z \rangle = 3.7$, and $\langle z \rangle = 2.7$, respectively.

In Figure 2, we show the number of H I lines of our sample at a given distance from the main components. The H I lines with relatively large column densities tend to cluster around the main components and have a symmetrical distribution, suggesting that they are related to each other. In contrast, the number of H I lines with smaller column densities decreases near the center of H I systems.

Therefore, we calculated $\xi(v)$ for some subsamples, varying the column density ranges. At first, a number of artificial lines matching the number of observed lines were randomly inserted

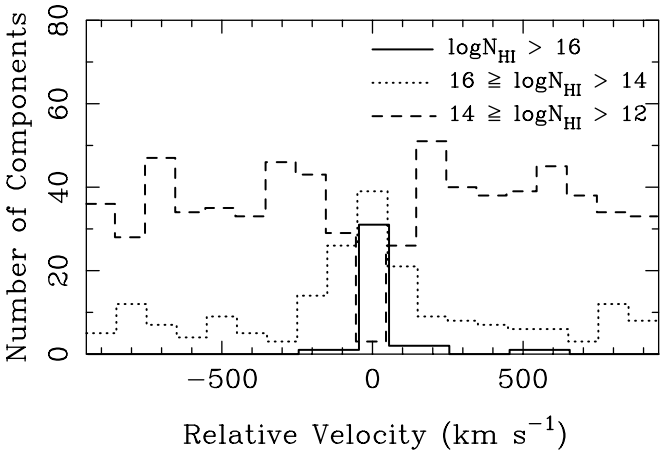

FIG. 2.—Distribution of 973 H I lines, including the main components, in 100 km s^{-1} wide bins from the main components.

into the 61 H I system windows. Since the observed H I systems always have main components at $v = 0$ km s^{-1}, we also placed an artificial line at the center of each system in order to produce unbiased simulated data. This process was repeated 250 times to obtain an average value for $N_{\rm exp}(v)$.

As a result of the analysis using all H I lines, we found that $\xi(v)$ shows a slight number excess at $\Delta v < 200$ km s^{-1}. The values of $\xi(v)$ for H I lines with various column density ranges in bins with a spacing of 50 km s^{-1} at 50 km s^{-1} $< v <$ 200 km s^{-1} are summarized in Table 1. Column (1) is the range of column density, columns (2), (3), and (4) are the values of $\xi(v)$ and 1 σ Poisson errors for velocity separations of 50–100, 100–150, and 150–200 km s^{-1}, respectively, and column (5) is the velocity width at which the lower 1 σ deviation of $\xi(v)$ first goes below $\xi(v) = 0$ over $v > 50$ km s^{-1}. Column (6) is the number of H I lines in each subsample. We see nonzero $\xi(v)$ at velocity separations of $v \sim 100$ km s^{-1} for weak H I lines and $v \sim 200$ km s^{-1} for strong H I lines. The correlation degree at $v = 50$–100 km s^{-1} was found to have a maximum for H I lines with $15 < \log N_{\rm H\,I} < 19$. This is one reason why we chose to use $\log N_{\rm H\,I} = 15$ as part of our definition of HDLs.

Within $\sim 0.5\ h^{-1}$ comoving Mpc of Lyman break galaxies (LBGs), the IGM contains less neutral hydrogen gas compared with the cosmologically averaged value at $z \sim 3$ (Adelberger et al. 2003). Some cosmological hydrodynamic simulations (e.g., Croft et al. 2002; Kollmeier et al. 2003) showed that this effect could be produced not by UV flux from the LBGs but by the galactic winds. This decreased absorption was detected in Adelberger et al. (2003) because the lines of sight to the quasars and the LBGs are different. In our spectra, strong H I lines (perhaps produced in the intervening galaxies) absorb most of the quasar flux within 50 km s^{-1} of their centers, which prevents us from detecting H I deficit in the vicinity of the strong H I lines.

4.2. *HDLs and LDLs*

We classified HDLs and LDLs with the following procedure. At first, we regarded all H I lines with $\log N_{\rm H\,I} > 15$ as HDLs, because the line clustering is stronger as $\log N_{\rm H\,I}$ increases, as Cristiani et al. (1997) found and we found above. However, we emphasize that the value of $\log N_{\rm H\,I} = 15$ is not strict. These strong H I lines may also be accompanied by weak H I lines that are physically associated with them. In fact, metal absorption lines sometimes have a core-halo structure: the strongest line is at the center of the absorption system, whereas the weak lines exist almost symmetrically on both sides of the strong one (e.g., Lu et al. 1996a; Prochaska et al. 2001; Misawa et al. 2003). Therefore, we defined a velocity distribution width for HDLs, $v_{\rm HDL}$. Since H I lines with relatively large column densities of $\log N_{\rm H\,I} = 13$–19, 14–19, 15–19, and 16–19 cm^{-2} are correlated with each other within the velocity separation of $v \sim 200$ km s^{-1}, we adopted $v_{\rm HDL} = \pm 200$ km s^{-1} and regard all H I lines with $12 < \log N_{\rm H\,I} < 15$, within 200 km s^{-1} of H I lines with $\log N_{\rm H\,I} > 15$ as HDLs. Hereafter we call the lines with $\log N_{\rm H\,I} < 15$ lying within 200 km s^{-1} of a $\log N_{\rm H\,I} > 15$ line "halo" HDLs to distinguish them from the original HDLs. Finally, all the 973 H I lines were separated into 306 HDLs (including halo HDLs) and 667 LDLs on the basis of these criteria.

4.3. *Column Density–Doppler Parameter Relation*

Using the subsamples of HDLs and LDLs, we investigated the correlation between the Doppler parameters and column densities. Our results are summarized in Figure 3.

In this figure, we also show lines with 5 km s^{-1} $< b <$ 15 km s^{-1}. We find 62 LDLs and 16 HDLs with $12 <$

TABLE 1

CLUSTERING PROPERTIES OF H I LINES

$\log N_{\rm H\,I}$ (cm^{-2}) (1)	ξ(50–100)[a] (2)	ξ(100–150)[a] (3)	ξ(150–200)[a] (4)	v[b] (km s^{-1}) (5)	n[c] (6)
12–19	0.17 ± 0.06	0.08 ± 0.05	0.11 ± 0.06	200	972
12–13	$0.52^{+0.28}_{-0.24}$	$0.16^{+0.25}_{-0.21}$	$-0.10^{+0.22}_{-0.18}$	100	244
12–14	0.32 ± 0.08	-0.00 ± 0.07	0.04 ± 0.07	100	716
12–15	0.21 ± 0.06	0.01 ± 0.06	0.06 ± 0.06	100	866
12–16	0.20 ± 0.06	0.05 ± 0.06	0.10 ± 0.06	100	933
13–19	0.19 ± 0.08	0.07 ± 0.07	0.15 ± 0.08	200	728
14–19	1.22 ± 0.30	$0.79^{+0.31}_{-0.27}$	$0.40^{+0.28}_{-0.24}$	200	256
15–19	$4.03^{+1.49}_{-1.17}$	$0.78^{+1.06}_{-0.70}$	$1.02^{+1.09}_{-0.74}$	200	106
16–19	$1.60^{+5.99}_{-2.15}$	$3.76^{+6.28}_{-3.08}$	$3.55^{+6.00}_{-2.94}$	200[d]	39

[a] Correlation and the 1 σ Poisson error for the velocity separations of 50–100, 100–150, and 150–200 km s^{-1}.

[b] Velocity width at which the lower 1 σ deviation of $\xi(v)$ first goes below $\xi(v) = 0$ over $v > 50$ km s^{-1}.

[c] Number of H I lines.

[d] We prefer to list $v = 200$ km s^{-1}, although the lower 1 σ deviation of $\xi(v)$ goes below $\xi(v) = 0$ at 50 km s^{-1} $\le v <$ 100 km s^{-1}; this could be due to the small sample.

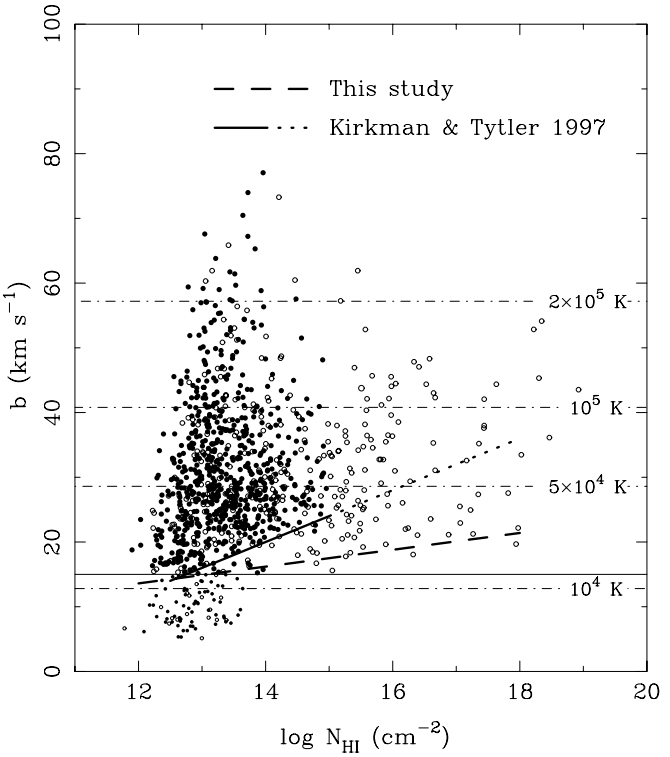

FIG. 3.—Doppler parameter vs. column density. Filled and open circles are LDLs and HDLs, respectively. LDLs and HDLs with $b < 15$ km s^{-1} are marked with small circles. The solid line is the relation between the column density $\log N_{\rm H\,I}$ and the minimum Doppler parameter $b_{\rm min}$ in KT97 ($12 < \log N_{\rm H\,I} < 15$), and the dotted line is the same relation extrapolated up to $\log N_{\rm H\,I} = 18$. The dashed line is the same relation for HDLs in our sample. The pure thermal Doppler parameters corresponding to the temperatures, $T = 10^4$, 5×10^4, 10^5, and 2×10^5 K, are shown with the thin dot-dashed horizontal lines.

$\log N_{\rm H\,I} < 14$ and 5 km s^{-1} $< b <$ 15 km s^{-1}, or 8% of the 973 LDLs and HDLs with $b > 15$ km s^{-1}. The proportion of HDLs to LDLs with $b < 15$ km s^{-1} ($16/62 = 25.8\%$) is similar to that for lines with $b > 15$ km s^{-1} and the same column density range ($142/583 = 24.4\%$). Since we did not identify metal lines, many of them could be metals, and since our spectra have a range of S/N ratios, many could be erroneous. Past studies that did consider these two effects found very few H I lines with these parameters (KT97; H95; L96). Hence, we ignore all lines with $b < 15$ km s^{-1}.

When we ignored H I lines with $b < 15$ km s^{-1}, we found a positive correlation between the minimum Doppler parameter, $b_{\rm min}$, and column density not only for LDLs approximately fitted by

$$b_{\rm min} = 4.0\log\left[\frac{N_{\rm H\,I}\ ({\rm cm}^{-2})}{10^{12.5}}\right] + 14.0\ {\rm km\ s}^{-1} \qquad (2)$$

at $12.5 < \log N_{\rm H\,I} < 15.0$ as seen in the past papers (e.g., KT97), but also for HDLs fitted by

$$b_{\rm min} = 1.3\log\left[\frac{N_{\rm H\,I}\ ({\rm cm}^{-2})}{10^{12.5}}\right] + 10.5\ {\rm km\ s}^{-1} \qquad (3)$$

at $12.5 < \log N_{\rm H\,I} < 19.0$. At $\log N_{\rm H\,I} > 15$, the HDLs often have b-values below the extrapolation of equation (2) for the LDLs. We, however, cannot compare the $b_{\rm min}$ values of LDLs with those of HDLs directly at $\log N_{\rm H\,I} > 15$, because there

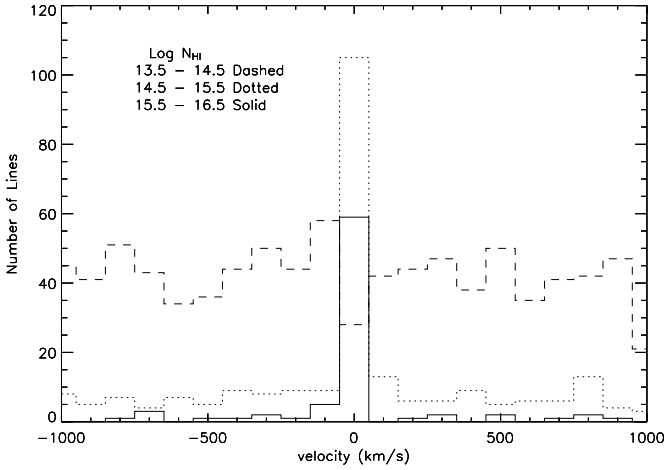

FIG. 4.—Same as Fig. 2, but for the hydrodynamic simulation. The column density ranges of the three subsamples are slightly different.

are no LDLs in that region. Nonetheless, if we look at the region of $\log N_{\rm H\,I} = 14$–15, a difference in the distribution of LDLs and HDLs is clear. At $\log N_{\rm H\,I} = 14$–15, only 2% (two of 91) LDLs are below the equation (2), whereas 20% (12 of 59) HDLs are located there. We do not think this difference is just a statistical accident. At $\log N_{\rm H\,I} < 14$, we do not see any remarkable difference between them, which could mean that there is little difference between the physical properties of LDLs and halo HDLs.

4.4. *Comparison with Simulation*

For weak H I lines, the correlation between column density and minimum Doppler parameter has already been reproduced by cold dark matter (CDM) simulations. Zhang et al. (1995) performed the hierarchical three-dimensional numerical simulation and found that the minimum b-value is increasing slightly with column density in a linear fashion. In order to mimic observational analysis more closely, Zhang et al. (1997) synthesized absorption spectra and extracted, deblended, and fitted the absorption features in generated spectra. The recovered data exhibit a $b_{\rm min}$ dependence on the column density well fitted by $b_{\rm min} = 5.5\log\left[N_{\rm H\,I}\ ({\rm cm}^{-2})/10^{12.5}\right] + 12.8$ km s^{-1}, which is consistent with the results of KT97 and our results for LDLs (eq. [2]) as shown in Figure 3.

We have performed a three-dimensional hydrodynamic simulation of Lyα clouds in a CDM-dominated universe and compared it with our observational results. We used the following input parameters: $\Omega_b = 0.04$, $\Omega_m = 0.30$, $\Omega_\Lambda = 0.70$, $H_0 = 70$ km s^{-1} Mpc^{-1}, $\sigma_8 = 0.73$, and power spectrum slope $n = 1$. We chose the size of the computational box to be $L = 0.7\,h^{-1}$ Mpc with the effective grid resolution of 256^3. We used the Haardt & Madau (1996) quasar spectrum with the photoionization rate $\gamma_{\rm H\,I} = (5.6\times10^{-13})(1+z)^{0.43}\exp\left[-(z-2.3)^2/1.95\right]$ ionizations per H I atom per second in the optical thin limit. Self-shielding is not included in the simulation. Figure 4 shows the number of H I lines at a given distance from the main component that are detected in our hydrodynamic simulation at $z = 2.9$–3.0 (similar figure to Fig. 2). The distribution of H I lines are examined for three column density ranges, $13.5 < \log N_{\rm H\,I} < 14.5$, $14.5 < \log N_{\rm H\,I} < 15.5$, and $15.5 < \log N_{\rm H\,I} < 16.5$. H I lines with relatively large column density, $\log N_{\rm H\,I} > 14.5$, tend to cluster around the main components. On the other hand, weaker H I lines show

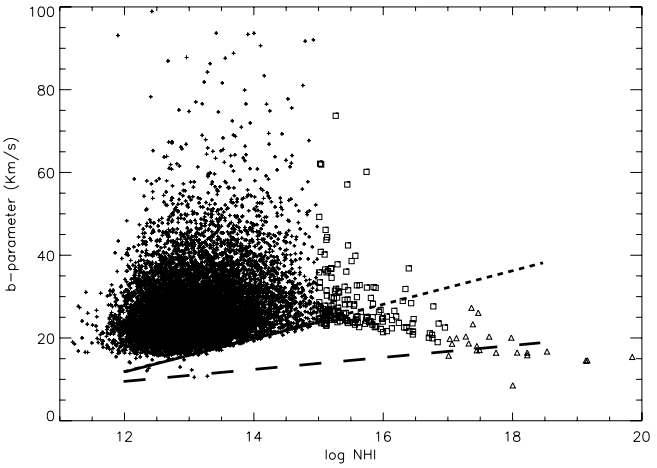

FIG. 5.—Similar to Fig. 3, but for the hydrodynamic simulation. Crosses are weak H I lines with $\log N_{\rm H\,I} < 15$. Open squares and triangles are completely deblended ($b < 40$ km s^{-1}) H I lines with column densities of $15 < \log N_{\rm H\,I} < 17$ and $\log N_{\rm H\,I} > 17$, respectively. In contrast with Fig. 3, we do not use the open squares for all lines within 200 km s^{-1} of lines with $\log N_{\rm H\,I} > 15$. The solid/dotted line and the dashed line denote the relations between $\log N_{\rm H\,I}$ and $b_{\rm min}$ for LDLs (eq. [2]) and HDLs (eq. [3]), respectively, from the observational results.

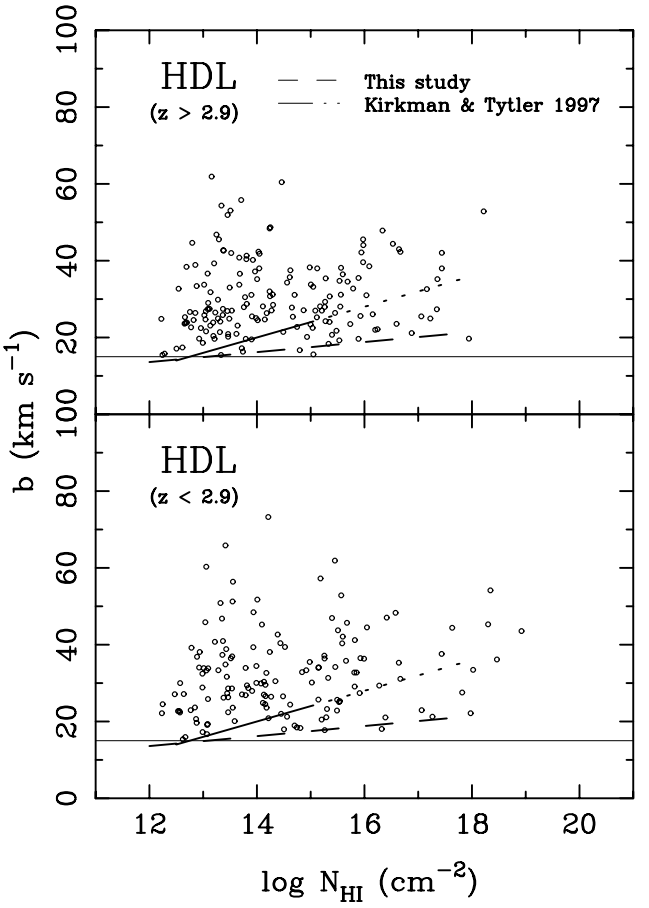

FIG. 6.—Doppler parameter vs. column density relation for HDLs at $z > 2.9$ and $z < 2.9$. We chose $z = 2.9$ when dividing the H I sample into two subsamples because it makes the numbers of H I systems in them nearly identical.

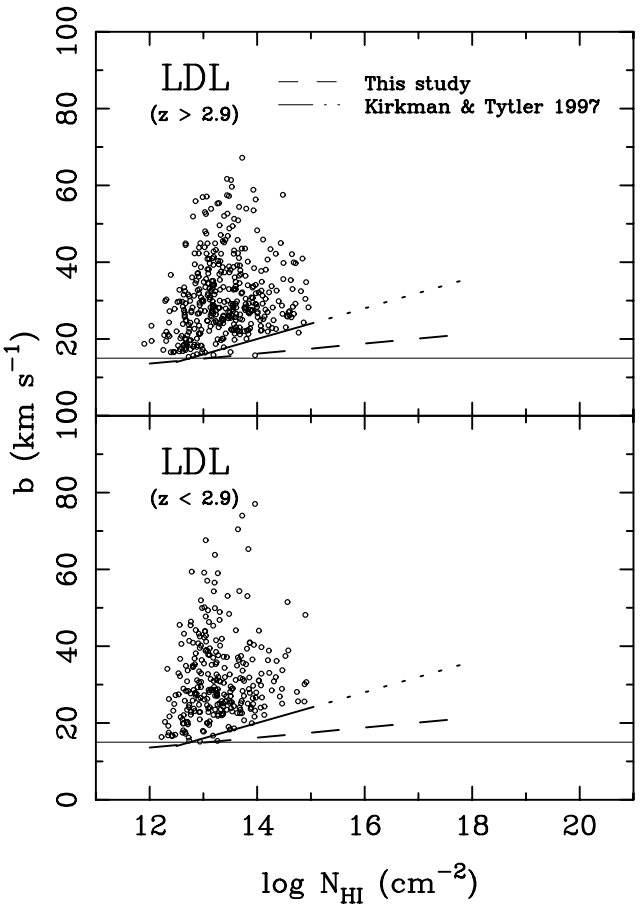

FIG. 7.—Same as Fig. 6, but for LDLs.

the decrease in their number near the main components. These trends are similar to those seen in the observation results, although the components with $14.5 < \log N_{\rm H\,I} < 15.5$ seem to be more concentrated in velocity in the simulated spectra.

In Figure 5, we show scatter plots between $\log N_{\rm H\,I}$ and b from the simulation. The difference of the distributions between HDLs and LDLs that we found in the observational result is successfully reproduced; strong HDLs with $\log N_{\rm H\,I} > 15$ have Doppler parameters smaller than the extrapolation of $b_{\rm min}$ for LDLs (eq. [2]).

One of the differences between the observation and the simulation is that there is a blank region at $\log N_{\rm H\,I} > 15$ and $b > 30$ km s^{-1} only in the simulation. It may be because absorption lines at the region in the observation are not completely resolved even with our improved fitting method (especially in the case that only a few orders of Lyman series are available) and have large b-values compared with the values that we might see with a very high S/N ratio. The minimum b-values, however, can be evaluated correctly even in such cases. On the other hand, the failure of the line deblending rarely happened in the simulation because we have not included noise in the synthetic spectra and because the resolution of our simulation, 256^3 by 0.7 h^{-1} Mpc ($\Delta x = 2.7$ kpc), is high enough compared with the minimum resolution ($\Delta x = 37.5$ kpc) necessary to evaluate appropriate b-values (Bryan et al. 1999).

Another difference is that few narrow HDLs, whose Doppler parameter is smaller than the value given by equation (2), are detected at $\log N_{\rm H\,I} < 15$ in the simulation (hereafter

"weak-narrow HDLs"). Here, we would like to emphasize that the b-values of H I lines near the strong H I absorbers could be overestimated in the simulation since we did not include self-shielding and shadowing effects that can be effective for the HDLs. We discuss this in the next section.

5. SUMMARY AND DISCUSSION

In this paper, we, for the first time, separated H I absorption lines into HDLs and LDLs, and we found differences between them using 40 quasar spectra. For weak H I lines (i.e., LDLs), the correlation between column density and the minimum Doppler parameter have often been investigated in both of the observation and the simulation. It is thought that this relation arises by virtue of the fact that higher column density clouds appear to be associated with denser regions in which the gas is adiabatically compressed and heated (e.g., Kim et al. 2001, 2002b). Kim et al. (2001, 2002b) also suggested that for weak H I lines the slope of the $\log N_{\rm H\,I}$–$b_{\rm min}$ relation became flatter as z decreased at $z > 3$, although there was no such significant trend at lower redshift $z \sim 2$. We, however, do not find any redshift evolution in our sample (Figs. 6 and 7).

The $\log N_{\rm H\,I}$–$b_{\rm min}$ relation for HDLs is clearly shallower than the extrapolated relations for weak H I lines in KT97 and Zhang et al. (1997), whereas the relation for LDLs is in good agreement with the past results. This means that HDL absorbers have relatively small Doppler parameters compared with the LDL absorbers at the same column density.

Davé et al. (1999) classify the H I gas clouds into three phases: (1) a cool low-density phase, (2) a shock-heated intermediate-density phase, and (3) a cold dense phase in galaxies. The first phase, with relatively low column densities of $\log N_{\rm H\,I} \leq 15$, makes the positive correlation between $\log N_{\rm H\,I}$ and $b_{\rm min}$, whereas the last phase with large column densities makes an anticorrelation.

When we think about H I clouds in the cold dense phase, the effect of radiative cooling must be taken into consideration. Such dense clouds with $\log N_{\rm H\,I} \geq 17$ (i.e., LLSs and DLA systems) can shield themselves against the background UV flux, which preserves more H I (i.e., shielding effect). A similar effect may happen in the low column density clouds if they are located near the high column density clouds (i.e., shadowing effect). These effects are important at least at $z \geq 6$ (Nakamoto et al. 2001), although they have not yet been evaluated quantitatively at lower redshift because of high complexity after the formation of the first stars and quasars. Zhang et al. (1995) also pointed out the importance of the shielding effect, although they did not include the effect in their simulation, nor did we here. If plenty of H I gas is preserved, the cooling of H I gas becomes very effective in regions in photoionization equilibrium (H I line cooling is the most effective cooling factor at $T \sim 10^4$ K), which could lower the temperature and decrease the value of the minimum Doppler parameter. Both of these effects tend to produce weak-narrow HDLs in the $\log N_{\rm H\,I}$–b plane, which makes the distribution of H I lines in the simulation more consistent with the observation for the HDLs.

We would like to acknowledge M. Chiba, R. Nishi, I. Murakami, M. Nagashima, and K. Okoshi, who gave us valuable comments on the theoretical interpretations. This work was supported in part by NASA grant NAG5-13113. We wish to thank the anonymous referee for the report, which improved the clarity of this presentation.

REFERENCES

Adelberger, K., Steidel, C. C., Shapley, A. E., & Pettini, M. 2003, ApJ, 584, 45
Barthel, P. D., Tytler, D. R., & Thomson, B. 1990, A&AS, 82, 339
Bryan, G. L., Machacek, M., Anninos, P., & Norman, M. L. 1999, ApJ, 517, 13
Burles, S. 1997, Ph.D. thesis, Univ. California, San Diego
Burles, S., Kirkman, D., & Tytler, D. 1999, ApJ, 519, 18
Burles, S., & Tytler, D. 1998a, ApJ, 499, 699
———. 1998b, ApJ, 507, 732
Carswell, R. F., Lanzetta, K. M., Parnell, H. C., & Webb, J. K. 1991, ApJ, 371, 36
Carswell, R. F., et al. 1996, MNRAS, 278, 506
Chen, H.-W., Lanzetta, K. M., Webb, J. K., & Barcons, X. 2001, ApJ, 559, 654
Churchill, C. W., & Vogt, S. S. 2001, AJ, 122, 679
Cristiani, S., D'Odorico, S., D'Odorico, V., Fontana, A., Giallongo, E., & Savaglio, S. 1997, MNRAS, 285, 209
Croft, R. A. C., Hernquist, L., Springel, V., Westover, M., & White, M. 2002, ApJ, 580, 634
Davé, R., Hernquist, L., Katz, N., & Weinberg, D. H. 1999, ApJ, 511, 521
Grogin, N. A., & Geller, M. J. 1998, ApJ, 505, 506
Haardt, F., & Madau, P. 1996, ApJ, 461, 20
Hu, E., Kim, T.-S., Cowie, L. L., Songaila, A., & Rauch, M. 1995, AJ, 110, 1526 (H95)
Kim, T.-S., Carswell, R. F., Cristiani, S., D'Odorico, S., & Giallongo, E. 2002a, MNRAS, 335, 555
Kim, T.-S., Cristiani, S., & D'Odorico, S. 2001, A&A, 373, 757
———. 2002b, A&A, 383, 747
Kirkman, D., & Tytler, D. 1997, ApJ, 484, 672 (KT97)
Kirkman, D., Tytler, D., Burles, S., Lubin, D., & O'Meara, J. M. 2000, ApJ, 529, 655
Kirkman, D., Tytler, D., Suzuki, N., O'Meara, J. M., & Lubin, D. 2003, ApJS, 149, 1
Kollmeier, J. A., Weinberg, D. H., Davé, R., & Katz, N. 2003, ApJ, 594, 75
Lanzetta, K. M. 1991, ApJ, 375, 1
Lanzetta, K. M., Bowen, D. V., Tytler, D., & Webb, J. K. 1995, ApJ, 442, 538
Lanzetta, K. M., Wolfe, A. M., Turnshek, D. A., Lu, L., McMahon, R. G., & Hazard, C. 1991, ApJS, 77, 1
Lu, L., Sargent, W. L. W., Barlow, T. A., Churchill, C. W., & Vogt, S. S. 1996a, ApJS, 107, 475
Lu, L., Sargent, W. L. W., Womble, D. S., & Takada-Hidai, M. 1996b, ApJ, 472, 509 (L96)
Lu, L., Wolfe, A. M., Turnshek, D. A., & Lanzetta, K. M. 1993, ApJS, 84, 1
McDonald, P., Miralda-Escudé, J., & Cen, R. 2002, ApJ, 580, 42
Misawa, T., Tytler, D., Iye, M., Kirkman, D., Suzuki, N., & Kashikawa, N. 2004, in preparation
Misawa, T., Yamana, T., Takada-Hidai, M., Wang, Y., Kashikawa, N., Iye, M., & Tanaka, I. 2003, AJ, 125, 1336
Nakamoto, T., Umemura, M., & Susa, H. 2001, MNRAS, 321, 593
O'Meara, J. M., Tytler, D., Kirkman, D., Suzuki, N., Prochaska, J. X., Lubin, D., & Wolfe, A. M. 2001, ApJ, 552, 718
Penton, S. V., Stocke, J. T., & Shull, M. 2002, ApJ, 565, 720
Péroux, C., Storrie-Lombardi, L. J., McMahon, R. G., Irwin, M., & Hook, I. M. 2001, AJ, 121, 1799
Petitjean, P., & Bergeron, J. 1994, A&A, 283, 759
Petitjean, P., Rauch, M., & Carswell, R. F. 1994, A&A, 291, 29
Petitjean, P., Webb, J. K., Rauch, M., Carswell, R. F., & Lanzetta, K. 1993, MNRAS, 262, 499
Pettini, M., Hunstead, R. W., Smith, L. J., & Mar, D. P. 1990, MNRAS, 246, 545
Pichon, C., Scannapieco, E., Aracil, B., Petitjean, P., Aubert, D., Bergeron, J., & Colombi, S. 2003, ApJ, 597, L97
Prochaska, J. X., et al. 2001, ApJS, 137, 21
Rauch, M. 1998, ARA&A, 36, 267
Rauch, M., Carswell, R. F., Chaffee, F. H., Foltz, C. B., Webb, J. K., Weymann, R. J., Bechtold, J., & Green, R. F. 1992, ApJ, 390, 387
Sargent, W. L. W., Steidel, C. C., & Boksenberg, A. 1988, ApJS, 68, 539
———. 1989, ApJS, 69, 703
Sargent, W. L. W., Young, P. J., Boksenberg, A., & Tytler, D. 1980, ApJS, 42, 41
Songaila, A., Cowie, L. L., Hogan, C. J., & Rugers, M. 1994, Nature, 368, 599
Songaila, A., Wampler, E. J., & Cowie, L. L. 1997, Nature, 385, 137
Steidel, C. C. 1990, ApJS, 74, 37
Steidel, C. C., & Sargent, W. L. W. 1992, ApJS, 80, 1

Storrie-Lombardi, L. J., McMahon, R. G., Irwin, M. J., & Hazard, C. 1996, ApJ, 468, 121
Tripp, T. M., Lu, L., & Savage, B. D. 1998, ApJ, 508, 200
Tytler, D. 1982, Nature, 298, 427
Tytler, D., Fan, X.-M., & Burles, S. 1996, Nature, 381, 207
Vogt, S. S., et al. 1994, Proc. SPIE, 2198, 362
Wampler, E. J., Williger, G. M., Baldwin, J. A., Carswell, R. F., Hazard, C., & McMahon, R. G. 1996, A&A, 316, 33
Webb, J. K. 1987, in IAU Symp. 124, Observational Cosmology, ed. A. Hewitt, G. Burbidge, & L. Z. Fang (Dordrecht: Reidel), 803
Young, P., Sargent, W. L. W., & Boksenberg, A. 1982, ApJS, 48, 455
Zhang, Y., Anninos, P., & Norman, M. L. 1995, ApJ, 453, L57
Zhang, Y., Anninos, P., Norman, M. L., & Meiksin, A. 1997, ApJ, 485, 496
Zhang, Y., Meiksin, A., Anninos, P., & Norman, M. L. 1998, ApJ, 495, 63